

## Coupling Between Precipitation and Contact-Line Dynamics: Multiring Stains and Stick-Slip Motion

Siddharth Maheshwari, Lu Zhang, Yingxi Zhu,\* and Hsueh-Chia Chang\*

Department of Chemical and Biomolecular Engineering, University of Notre Dame, Notre Dame, Indiana 46556, USA

(Received 29 March 2007; published 28 January 2008)

The contact line in an evaporating drop can stay pinned to form a single ring or can shrink in a discontinuous stepwise manner and generate multiple rings. We demonstrate the latter with DNA solutions and attribute it to a pinning-depinning cycle that generates new contact lines. The new contact line recedes after depinning and is repinned at an internal precipitate ring that determines the location of the next contact line. Each precursor ring is formed when DNAs are trapped by an internal microstagnation flow and precipitation dynamics hence control this unsteady drop motion.

DOI: [10.1103/PhysRevLett.100.044503](https://doi.org/10.1103/PhysRevLett.100.044503)

PACS numbers: 47.54.-r, 47.55.N-, 47.55.np, 68.08.Bc

Drying of suspensions is an everyday phenomenon, which although easily observable, gives rise to surprisingly rich morphologies, based on the exact evaporation geometry, solute size and chemistry, and substrate-solvent interaction [1–4] and is proving to be an important small scale fabrication process [5,6]. The formation of the well-known coffee-stain pattern for the case of an evaporating drop with a pinned contact line is the result of an evaporative flux directed towards the pinned contact line, which carries the solute and deposits it near the contact line to form a single ring [7–10]. In contrast, though there have been reports of multiring formation [11–16], the mechanism behind multiple rings formed via pinning-depinning contact-line dynamics is not well understood. Here we find that contact-line hydrodynamics are dictated by precipitation dynamics for multiring formation.

The one-ring pattern formation process requires the contact line to be pinned on to the substrate at a nonzero contact angle for the entire cycle, while evaporation of the solvent, which is maximum at the contact line, transports the solute outwards and towards the pinned contact line. This causes the formation of the ringlike stain at the outer regions of the drop. At the same time, sustained evaporation and the pinning of the contact line causes the drop height to continually decrease. Ultimately when the meniscus at the center of the original drop comes in contact with the solid substrate, the meniscus ruptures at that point and almost instantaneously the entire drop dewets and the stain-formation process is completed. The notable feature of this process is the almost 100% transfer of the solute to the contact line, pointing to the pinning of the contact line at its initial position throughout the entire cycle. In contrast, the multiring pattern requires repeated pinning and depinning of the contact line.

We use  $\lambda$ -DNA (Sigma, 115 kilo-base pairs,  $M_n = 76\,000$  kDa) fluorescent labeled with YOYO-1 (Invitrogen,  $\lambda_{ex} = 491$  nm/ $\lambda_{em} = 509$  nm), dissolved in deionized water with 1 mM EDTA. The glass coverslips (Fisher) used in this study were cleaned by soaking over-

night in piranha solution (70%  $H_2O_2$  and 30%  $H_2SO_4$ ) and then washed with purified deionized water (Barnstead NanoPure). The stock DNA solution was then diluted to solutions with concentrations ranging from 50 to 0.05  $\mu\text{g/mL}$ . The solution was transferred onto the clean glass surface from a micropipette. The volume of the drops ranged from 0.5 to 20  $\mu\text{L}$  and the temperature from 22 to 40  $^\circ\text{C}$ . The temperature was controlled with an accuracy of  $\pm 0.5$   $^\circ\text{C}$  during the experimental process to ensure a constant evaporation rate. A confocal laser scanning microscope (Zeiss LSM Pascal 5) was used to observe the stain patterns obtained during and after evaporation. For *in situ* dynamic measurements, fluorescent micrographs in time sequence were recorded during evaporation to characterize the different steps in the redistribution of DNA molecules during the evaporation process [17]. The contact angle of the drops during evaporation was measured by a contact-angle goniometer (Ramé-hart 100-F0).

We use aqueous solution of DNA as it precipitates readily near the surface and allows high-resolution imaging with fluorescent tags [18]. Figure 1 depicts the observed multiring stain patterns at different DNA concentrations, the most important single parameter influencing stain formation. Three kinds of stain-formation dynamics are observed and are delineated in the temperature-concentration phase diagram of Fig. 2(a). At high (region I) and intermediate (region II) DNA concentrations, rupture or depinning of the liquid film near the contact line is observed prior to the formation of the next ring. A new contact line is created during the rupture event and recedes very rapidly inward until it is pinned at a new position. These events repeat for each successive ring formation and exhibit a stepwise contact-line motion with a clear pinning interval and a receding interval, shown in Fig. 2(b). Although both subregimes exhibit similar pinning-depinning sequence, the variation in DNA concentration causes some observable differences in the ring spacing, with region I having smaller spacing and less sensitivity to the DNA concentration, as well as a shorter

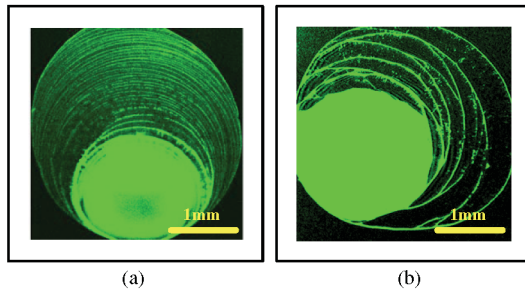


FIG. 1 (color). Typical DNA stain patterns with multiring formation. (a) Stain pattern at high concentration  $\sim 50 \mu\text{g/ml}$  for a  $3 \mu\text{l}$  drop. Note the regularity of the stain pattern and the uniformity in ring spacing. (b) Similar multiring formation at intermediate concentration  $\sim 25 \mu\text{g/ml}$  for a  $3 \mu\text{l}$  drop. Dewetting is evident and the ring spacing is larger.

pinning interval. At low DNA concentrations in region III, this pinning-depinning of the contact line is replaced by a smooth recession of the original contact line with deposits formed at some intervals. Here the behavior is dramatically different from regions I and II and the contact-line dynamics do not involve rupture or depinning of the liquid film and creation of new contact lines. Rather, the recession of the original contact line is very smooth, as documented in Fig. 2(b), and the formation of multirings, if any, is quite random and periodic multiple rings are generally not present. In this Letter we focus on the discontinuous pinning-depinning mechanism at high and intermediate concentrations of regions I and II, where an apparent stick-slip dynamics has been endowed by the rupturing and pinning sequence. It should be noted that the observed mechanism is quite different from “fluid fixation” behavior, i.e., stretching DNA in the flow field generated by an evaporating drop and immobilizing them on charged surfaces [19], although we have observed some stretching of

DNA molecules within successive rings. Fluid fixation behavior was generally observed at low concentrations. It should also be noted that pattern formation via DNA droplet drying is quite rich and can yield a variety of stain patterns [20], but in this Letter we focus on multiple ring formation only. Additionally, consistent with previous reports [15] we have also seen multirings with small ( $\sim 0.5 \mu\text{m}$ ) polystyrene colloidal suspensions and they show similar dynamics as DNA multiring formation.

The ring wavelength  $\lambda$  was found to decrease with increasing DNA concentration in regions I and II, as shown in Fig. 2(c), where the average wavelength for a given drop is reported along with its initial DNA concentration. Similar wavelength-concentration dependence is observed at different temperatures, indicating that precipitation plays an important role in this process. Drops with dimension as small as  $200 \mu\text{m}$ , which is much smaller than the capillary length ( $\sqrt{\sigma/\rho g} \sim 2.7 \text{ mm}$ , where  $\sigma$  is the surface tension,  $\rho$  the density, and  $g$  the acceleration due to gravity), showed similar stain patterns as those in drops much larger. The smallest drops were produced by electrospraying. The variation in wavelength with the drop volume has been quantified in the inset of Fig. 2(c), showing an asymptote beyond a critical drop volume. We observed similar multiring stains on amine-terminated self-assembled monolayers on glass [21] as well as on silicon wafers (rms roughness  $< 0.5 \text{ nm}$ ). These observations suggest a generic mechanism for multiring formation process independent of evaporation rate, drop volume and nano-scale surface roughness, but sensitive to drop concentration and hence precipitation dynamics.

The regular stain patterns in regions I and II suggest a similar precipitation mechanism for successive ring formation. Initially the contact line is pinned at its original location and evaporation drives an outward radial flux in

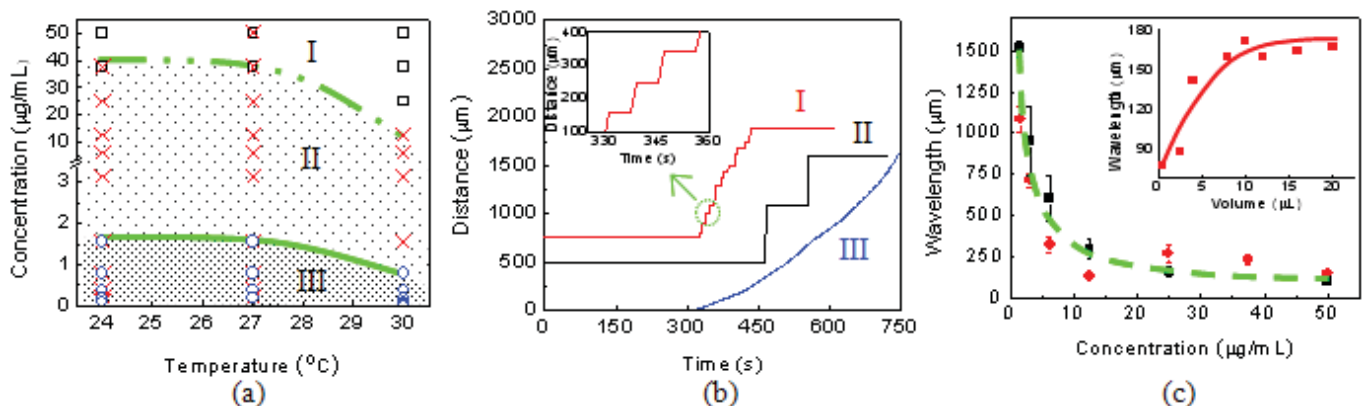


FIG. 2 (color). Three regions for stain patterns and formation dynamics. (a) Concentration-temperature phase diagram for DNA evaporation, subdivided into three regions I, II, III. The subdivision approximately follows the concentration variation, with region I at high concentration, region II at intermediate concentration, and region III at low concentration. (b) Contact-line position as a function of time, for different regions. The steplike motion with a clear pinning interval and a receding interval is evident for regions I and II. For region III, the recession of the original contact line is very smooth. For clarity, the profiles for regions I and II have been shifted upwards. (c) Variation of wavelength with concentration, at  $24^\circ\text{C}$  (red) and  $30^\circ\text{C}$  (black), indicating an inverse proportionality. Inset: Variation in wavelength with drop volume, showing an increase and then approaching an asymptote.

the drop that deposits DNA at the contact line forming the outermost ring, similar to coffee-stain formation. This pinning and evaporation also cause the drop height to decrease making the drop approach a pancake shape, which is consistent with the observation of a constant asymptote for the ring wavelengths at larger drop volumes; it suggests that the drop profile has become flat such that the contact-line dynamics are decoupled from the drop interior and that the multiring formation process is insensitive to the drop size.

The contact line does not remain pinned at any location for the entire duration. We attribute the contact-line dynamics to precipitation in the drop interior which occurs before the contact line slips. Internal concentration and precipitation of solute into a ring, without templating by surface functionalization, can only occur if driven by a microflow with a ring structure. Converging stagnation flows on the surface are particularly effective in solute concentration at the stagnation region. Such flows can sweep the solute to a locus and weak viscous drag at the stagnation region cannot resuspend them into the bulk if a substrate-solute attractive force is present. In our case, a slight DNA affinity for the substrate is sufficient to trap the DNA molecules swept towards the stagnation line. In other similar cases, electro-osmotic and electrohydrodynamic surface stagnation flows have been used to concentrate and assemble bacteria [22,23].

The appearance of this stagnation flow and precipitation at the stagnation line away from the contact line is evident from the fluorescence of the DNA molecules in Fig. 3(a), which show a maximum away from the contact line. The locus of maximum intensity moves inward initially, but becomes immobilized at a specific location within the drop as the intensity increases. The existence of the inner ring is also supported by the appearance of miscible viscous fingers shown in Fig. 3(b), which occurs when a less viscous fluid is pushing against a more viscous fluid [24]. This clearly indicates a viscosity maximum away from the contact line, and, as the viscosity of the DNA solution is a strong function of the concentration, precipitation of DNA away from the contact line. This local zone of high concentration pins the receding contact line created during rupture and hence determines the location of the new contact line. Fingering also creates an approximate square wave pattern on the stains because of depletion of the deposits near the contact line which creates partial or total gaps on the rings as well as triangular deposits between rings. The dynamics of the stain-formation process can be clearly seen in the supplementary section.

The pinning of the receding contact line is documented by a sequence of images in Fig. 3(a) (i)–(iii) [17]. The location of this internal ring is estimated by the highest DNA concentration (fluorescent intensity). Subsequent images clearly show that the receding contact line is pinned near the marked contour during the formation of two successive rings. This internal precipitation ring region is the precursor for the new contact line.

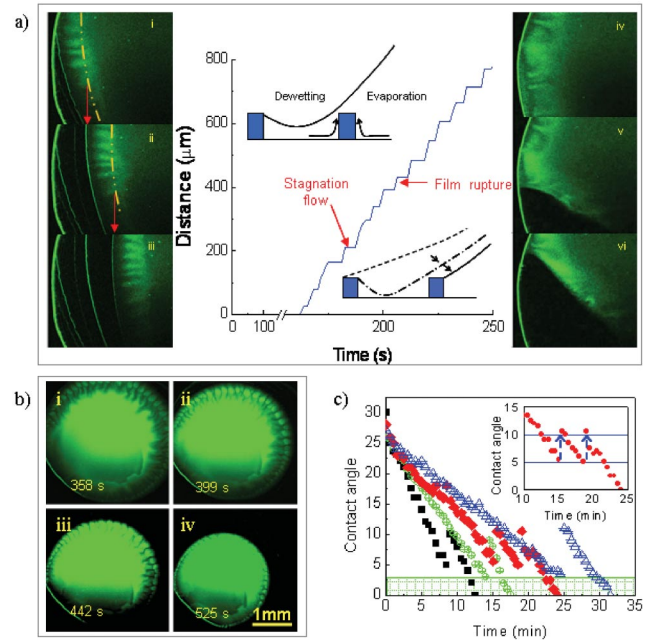


FIG. 3 (color). Motion of the contact line. (a) Typical receding dynamics for the contact line, similar to a staircase pattern. The horizontal part of the staircase indicates pinned contact line, when the stagnation flow occurs to create the internal ring. Pinning is documented by a sequence of images (i)–(iii). The location of this internal ring is estimated by the highest DNA concentration (fluorescent intensity), and it can be seen that the next ring forms very close to this position. The inclined part shows the depinning of the contact line via rupture of the annular film between two successive rings, and the contact line moves from the peripheral ring to the internal ring as shown in (iv)–(vi). (b) Miscible viscous fingering pattern in a drop with DNA concentration  $50 \mu\text{g/ml}$ . Successive images are taken at 358, 399, 442, and 525 seconds after evaporation begins. (c) Contact-angle variation during typical evaporation sequence, for different drop volumes: (black)  $4 \mu\text{l}$ , (green)  $8 \mu\text{l}$ , (red)  $12 \mu\text{l}$ , and (blue)  $16 \mu\text{l}$ . The shaded portion near the time axis represents uncertainty in measurement due to very small angles.

The existence of a surface stagnation flow within the evaporating drop leading to precipitation of DNA at the stagnation region is documented in Fig. 3(a), and here we propose a flow field to explain this stagnation flow. After the pancake shaped drop develops, continued evaporation causes the curvature near the contact line to change from concave downwards to concave upwards. This dimple is developed when considerable precipitation occurs at the contact line to form a concentrated deposit. As such, the contact line is not pinned to the substrate but is rather at an elevated position on the vertical wall of the DNA precipitate ring. As the solution wets the precipitate, the interface changes its convex curvature at the edge of the drop to a concave one near the precipitate, the dimple is hence formed near the contact-line precipitate. Such a dimpled fluid interface under evaporation has been reported previously [14]. The dimple can reduce the local film thickness to below  $1 \mu\text{m}$  and cause a local dewetting flow away from



the dimple, mostly in the inward direction, because of larger film thickness. This inward flow and the outward evaporation flow changes the flow behavior near the contact line and form a stagnation ring some distance away from the original contact line as shown in Fig. 3(a). With continuous dewetting flux from the dimple, the meniscus comes closer and closer to the substrate and once it touches the substrate, an abrupt rupture occurs. This event between two successive rings produces a new contact line that then moves rapidly to the inner ring. In fact, the occurrence of rupture, as shown in Fig. 3(a) (iv)–(vi), clearly points to the presence of a dimple near the contact line, because for rupture to occur, the liquid surface must come in contact with the solid substrate underneath, which can only occur when the curvature near the contact line changes and becomes concave upwards.

Macroscopically, this sequence of events produces an apparent stick-slip behavior with oscillatory changes in contact angle, as is evident in the contact-angle measurements in Fig. 3(c). The contact-angle fluctuations are observed for the first few rings in region II before the film thickness becomes too thin to allow an accurate measurement of the contact angle. These are manifestations of rupturing with successive creation of new contact lines.

The rupture event leaves behind an annulus of liquid which contains the precipitate ring of the previous generation. This separated annular liquid volume evaporates to leave behind the stain rings. As the DNAs in the annular liquid volume are mostly in the precipitate ring, which does not redissolve into the liquid, the stain width is expected to be close to the width of the internal precipitate ring. The scaling for the stain spacing in Fig. 2(c) can then be explained with a simple mass balance model. Assuming  $\Delta x$  to be the width of precipitate ring at the stagnation ring, a 1D flux balance leads to

$$\Delta x \frac{\partial C}{\partial t} = r_e C_\infty, \quad (1)$$

where,  $C$  and  $C_\infty$  are the DNA concentrations in the ring region and the bulk, respectively,  $t$  the time, and  $r_e$  the local evaporative flux. We can obtain a scaling relation from the above equation,  $C_m \sim r_e C_\infty \tau / \Delta x$  where  $C_m$  is the maximum concentration of DNA achieved when DNA molecules aggregate to form ring precursors in time scale  $\tau$ . This critical concentration is related to the DNA precipitate concentration or the DNA concentration when the solution viscosity becomes so large that the trap becomes immobile. Consequently, spacing between two successive rings is given by:  $\lambda \approx r_e \tau \approx \Delta x C_m / C_\infty$ , which is independent of drop size or evaporation rate for large drops under the experimental conditions, but inversely proportional to bulk DNA concentration, as shown in Fig. 2(c).

Hence we conclude that internal precipitation at surface stagnation points regulates contact-line recession of thin

films, which has important ramifications for evaporative pattern formation. Microscale heterogeneities via surface functionalization, flow instabilities, roughness or artificial templating can produce microflows with different topologies and stagnation loci, which can, in turn, lead to stains and precipitates with exceptionally rich morphologies. Combined with the condensation of large molecules that form networks or scaffolds, such precipitate structures can be very useful for micro-fabrication and self-assembly processes.

The authors thank Timothy P. Kegelman for experimental assistance. This work was supported (L. Z. and Y. Z.) by the Donors of the ACS Petroleum Research Fund (Grant No. 45063-G9) and NSF (Grant No. CBET06-51408), and (S. M. and H.-C. C.) by NSF and NASA.

---

\*yzhu3@nd.edu, hchang@nd.edu

- [1] J. Xu *et al.*, Phys. Rev. Lett. **96**, 066104 (2006).
- [2] Z. Neda *et al.*, Phys. Rev. Lett. **88**, 095502 (2002).
- [3] V. X. Nguyen and K. J. Stebe, Phys. Rev. Lett. **88**, 164501 (2002).
- [4] M. Abkarian, J. Nunes, and H. A. Stone, J. Am. Chem. Soc. **126**, 5978 (2004).
- [5] N. Rana and S. T. Yau, Nanotechnology **15**, 275 (2004).
- [6] D. J. Harris *et al.*, Phys. Rev. Lett. **98**, 148301 (2007).
- [7] R. D. Deegan *et al.*, Nature (London) **389**, 827 (1997).
- [8] R. D. Deegan *et al.*, Phys. Rev. E **62**, 756 (2000).
- [9] B. Rieger, L. R. van den Doel, and L. J. van Vliet, Phys. Rev. E **68**, 036312 (2003).
- [10] Y. O. Popov, Phys. Rev. E **71**, 036313 (2005).
- [11] E. Adachi, A. S. Dimitrov, and K. Nagayama, Langmuir **11**, 1057 (1995).
- [12] H. Maeda, Langmuir **15**, 8505 (1999).
- [13] R. D. Deegan, Phys. Rev. E **61**, 475 (2000).
- [14] P. Takhistov and H. C. Chang, Ind. Eng. Chem. Res. **41**, 6256 (2002).
- [15] L. Shmuylovich, A. Q. Shen, and H. A. Stone, Langmuir **18**, 3441 (2002).
- [16] Z. Q. Lin and S. Granick, J. Am. Chem. Soc. **127**, 2816 (2005).
- [17] See EPAPS document No. E-PRLTAO-100-037803 for videos showing three stain-formation regions. For more information on EPAPS, see <http://www.aip.org/pubservs/epaps.html>.
- [18] I. I. Smalyukh *et al.*, Phys. Rev. Lett. **96**, 177801 (2006).
- [19] J. Jing *et al.*, Proc. Natl. Acad. Sci. U.S.A. **95**, 8046 (1998).
- [20] X. H. Fang *et al.*, Langmuir **22**, 6308 (2006).
- [21] M. Mrksich *et al.*, Proc. Natl. Acad. Sci. U.S.A. **93**, 10775 (1996).
- [22] J. Wu *et al.*, Ind. Eng. Chem. Res. **44**, 2815 (2005).
- [23] D. Hou, S. Maheshwari, and H. C. Chang, Biomicrofluidics **1**, 014106 (2007).
- [24] Y. X. Ben, E. A. Demekhin, and H. C. Chang, Phys. Fluids **14**, 999 (2002).